J. Fluid Mech. (2005), *vol.* 531, *pp.* 325–334. © 2005 Cambridge University Press
doi:10.1017/S002211200500399X Printed in the United Kingdom

Stability of flow through a slowly diverging pipe

By KIRTI CHANDRA SAHU AND RAMA GOVINDARAJAN

Engineering Mechanics Unit, Jawaharlal Nehru Centre for Advanced Scientific Research, Bangalore 560 064, India
rama@jncasr.ac.in

(Received 24 August 2004 and in revised form 11 February 2005)

Although the critical Reynolds number for linear instability of the laminar flow in a straight pipe is infinite, we show that it is finite for a divergent pipe, and approaches infinity as the inverse of the divergence angle. The velocity profile at the threshold of inviscid stability is obtained. A non-parallel analysis yields linear instability at surprisingly low Reynolds numbers, of about 150 for a divergence of 3°, which would suggest a role for such instabilities in the transition to turbulence. A multigrid Poisson equation solver is employed for the basic flow, and an extended eigenvalue method for the partial differential equations describing the stability.

1. Introduction

The laminar flow through a straight pipe is linearly stable for any Reynolds number (Davey & Drazin 1969; Lessen, Sadler & Liu 1968), but, as first demonstrated by Reynolds (1883), transition to turbulence usually occurs at a Reynolds number Re, based on the pipe diameter and mean velocity, of around 2000. By reducing the external disturbances, it is possible to achieve laminar flow up to $Re \sim 10^5$ (Huerre & Rossi 1998) when the pipe is smooth and the flow at the inlet very quiet. The Reynolds number up to which it is possible to keep the flow laminar varies inversely with the level of external disturbance (Hof, Juel & Mullin 2003). Although questions remain about the complete route to turbulence in a straight pipe, it seems likely that the spectrum of linear (stable) modes has a role to play via transient algebraic growth (Meseguer & Trefethen 2003; Schmid & Henningson 1994) of disturbances. It has recently been demonstrated both theoretically and experimentally that a nonlinear self-sustaining mechanism leads to the existence of travelling waves (and time-periodic states) that appear to play a key role in shear turbulence (Faisst & Eckhardt 2003, 2004; Hof *et al.* 2004; Waleffe 1998, 2001).

Our purpose in this paper is to examine the possible role of small local divergences in the transition process. These could have a large effect since linear stability is described by a singular perturbation problem. Whereas a large amount of work has been done on the flow in significantly converging/diverging (e.g. Floryan 2003) and in suddenly expanding geometries, we know of no work on the stability of *slowly* diverging pipe flows. Sudden expansions have attracted attention because of the recirculation zone they generate. In particular, Fearn, Mullin & Cliffe (1990) and Cherdron, Durst & Whitelaw (1978) study the length of the recirculation zone as a function of the Reynolds number, and Sreenivasan & Strykowski (1983) examine the oscillations of the recirculating bubble and their effect on the flow. Our focus is different. Eagles (1965) and Eagles & Weissman (1975), analysed the Jeffery–Hamel flow generated by a slowly diverging channel, and showed by linear parallel stability

https://doi.org/10.1017/S002211200500399X Published online by Cambridge University Press

analysis (the Orr–Sommerfeld equation), that the critical Reynolds number decreases by a large amount even for a small divergence angle. The divergent *pipe* is more interesting for several reasons: the critical Reynolds number is infinite for an angle of divergence of zero, the Reynolds number is a decreasing function of the streamwise (axial) coordinate x, and the flow non-parallelism is larger for a given divergence. Here, we employ a two-pronged approach. For the mean flow, we derive an axisymmetric Jeffery–Hamel equation (AJH), which is valid at small divergence angles. At larger divergence angles (1° or greater) we solve the Navier–Stokes equations directly in the axisymmetric geometry shown in figure 1, with a divergent portion of finite extent. At small divergence angles and high Reynolds numbers (above 1000), a parallel flow stability analysis is conducted on the AJH profile, while at lower Reynolds numbers, the partial differential equations for non-parallel stability are solved as an extended eigenvalue problem.

2. The basic flow

2.1. *Axisymmetric Jeffery–Hamel equation*

We begin by noting that unlike in a divergent two-dimensional channel, no similarity flow is possible in a divergent pipe. At very low angles of divergence, however, it is possible to derive a one-parameter family of velocity profiles, where the parameter

$$S \equiv aRe \tag{2.1}$$

varies slowly in the axial coordinate x. Here the slope

$$a \equiv \frac{\mathrm{d}R(x_d)}{\mathrm{d}x_d} \ll 1, \tag{2.2}$$

R is the radius of the pipe, and the subscript d stands for a dimensional quantity. Upon eliminating the pressure from the axisymmetric momentum equations, we obtain

$$-\frac{V_d}{r_d}\frac{\partial U_d}{\partial r_d} + U_d\frac{\partial^2 U_d}{\partial x_d \partial r_d} + V_d\frac{\partial^2 U_d}{\partial r_d^2} - \nu\left[\frac{\partial^3 U_d}{\partial r_d^3} - \frac{1}{r_d^2}\frac{\partial U_d}{\partial r_d} + \frac{1}{r_d}\frac{\partial^2 U_d}{\partial r_d^2}\right] = 0, \tag{2.3}$$

where ν is the kinematic viscosity, and r is the radial coordinate. The axial and radial velocities, U_d and V_d respectively, may be written in terms of a generalized streamfunction Ψ_d as

$$U_d = \frac{1}{r_d}\frac{\partial \Psi_d}{\partial r_d}, \qquad V_d = -\frac{1}{r_d}\frac{\partial \Psi_d}{\partial x_d}, \tag{2.4}$$

to satisfy continuity. Substituting this in equation (2.3), we obtain

$$\begin{aligned} 3r_d\frac{\partial \Psi_d}{\partial x_d}\frac{\partial^2 \Psi_d}{\partial r_d^2} - 3\frac{\partial \Psi_d}{\partial r_d}\frac{\partial \Psi_d}{\partial x_d} + r_d^2\frac{\partial \Psi_d}{\partial r_d}\frac{\partial^3 \Psi_d}{\partial r_d^2 \partial x_d} - r_d\frac{\partial \Psi_d}{\partial r_d}\frac{\partial^2 \Psi_d}{\partial r_d \partial x_d} - r_d^2\frac{\partial \Psi_d}{\partial x_d}\frac{\partial^3 \Psi_d}{\partial r_d^3} \\ - \nu\left[r_d^3\frac{\partial^4 \Psi_d}{\partial r_d^4} - 2r_d^2\frac{\partial^3 \Psi_d}{\partial r_d^3} + 3r_d\frac{\partial^2 \Psi_d}{\partial r_d^2} - 3\frac{\partial \Psi_d}{\partial r_d}\right] = 0. \end{aligned} \tag{2.5}$$

The above equation is non-dimensionalized using the local radius $R(x_d)$ and the centreline velocity $U_c(x_d)$ as scales, e.g. $\Psi_d = U_c R^2 \Psi$. In particular,

$$\mathrm{d}x_d = R\,\mathrm{d}x. \tag{2.6}$$

The Reynolds number is assumed to be high and the divergence small enough that all terms of $O(Re^{-2})$ or $O(a^2)$ and higher are negligible. The resulting equation in

https://doi.org/10.1017/S002211200500399X Published online by Cambridge University Press

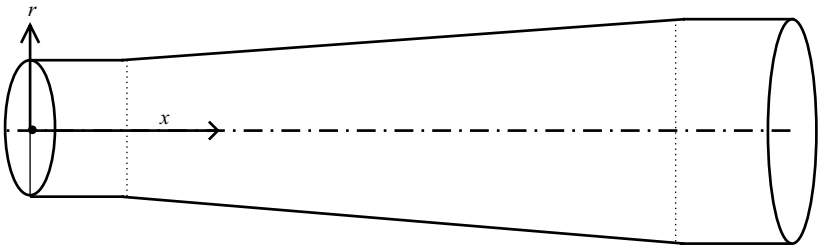


FIGURE 1. Schematic of the divergent pipe used in the numerical simulations; not to scale.

non-dimensional form becomes

$$[q\Psi - ra\Psi'][-3\Psi' + 3r\Psi'' - r^2\Psi'''] - r\Psi'[q\Psi' - r\Psi''a - \Psi'a] + r^2\Psi'$$
$$[(q-2a)\Psi'' - ra\Psi'''] - \frac{1}{Re}\left[r^3\Psi^{\mathrm{iv}} - 2r^2\Psi''' + 3r\Psi'' - 3\Psi'\right] = 0, \qquad (2.7)$$

where

$$q \equiv \frac{1}{U_c R^2}\frac{\mathrm{d}}{\mathrm{d}x_d}(U_c R^2),$$

the Reynolds number is defined as $Re(x_d) \equiv U_c(x_d)R(x_d)/\nu$, and the primes refer to differentiation with respect to r. For the case of near-similar flow, given constant mass flow rate, we may set $q = 0$, and (2.7) may be integrated once with respect to r to give

$$r^2U''' = -rU'' + (1 - 4Sr^2U)U', \qquad (2.8)$$

where $U = \Psi'/r$. The boundary conditions are $U = 0$ at $r = 1$, and $U = 1$, $U' = 0$ at $r = 0$. Profiles obtained from equation (2.8) are compared to those obtained from a numerical axisymmetric Navier–Stokes solution in the following subsection.

2.2. *Numerical solution*

The geometry studied here is as shown in figure 1, with a straight pipe at the entry, followed by an axisymmetric divergent portion, which in turn is followed by a long straight exit portion. The length and velocity scales, redefined for convenience in this subsection alone, respectively are the radius R_i and the centreline velocity U_i at the inlet. In the case presented here, the divergent portion starts at $x = 9.4$ and ends at $x = 91$ with a 3° angle of divergence. The total length of the domain is $L = 120$. The axisymmetric Navier–Stokes equations for steady, incompressible, Newtonian flow in the streamfunction–vorticity formulation, in non-dimensional form, are given by

$$\frac{\partial \Omega}{\partial t} + (\boldsymbol{U}\cdot\nabla)\Omega = \frac{1}{Re_i}\nabla^2\Omega, \qquad (2.9)$$

$$\Omega = -\nabla^2\Psi, \qquad (2.10)$$

where $Re_i \equiv U_iR_i/\nu$, $\Omega(x, r)$ is the azimuthal vorticity, $\boldsymbol{U}$ is the velocity vector, and t is time. The boundary conditions at the centreline are $\Psi = \Omega = V = \partial U/\partial r = 0$. No-slip and impermeable boundary conditions are imposed at the wall. At the inlet, a parabolic velocity profile is prescribed. The reason for using a long exit section, and the consequent increase in computational effort, is due to the requirement that the Neumann boundary conditions $\partial\Psi/\partial x = 0$ be valid at the exit. We begin with a guess solution: a parabolic velocity profile at every axial location, and march in psuedo-time until a steady-state solution is obtained. The vorticity distribution at

https://doi.org/10.1017/S002211200500399X Published online by Cambridge University Press

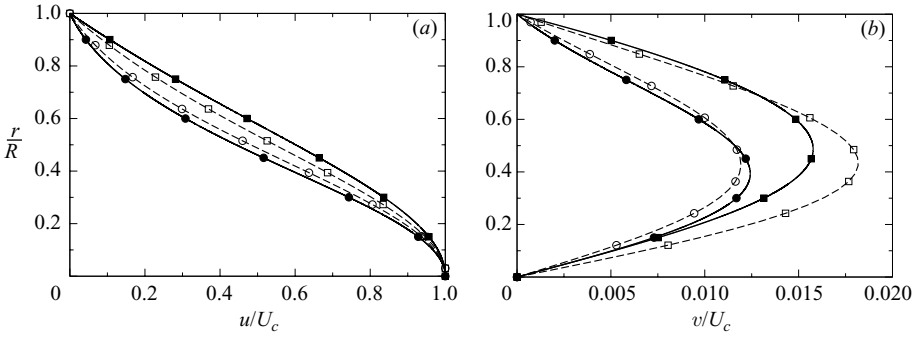


FIGURE 2. Comparison of numerically obtained velocity profiles (solid lines) at different axial locations (circles: $x = 22.9$, $S = 7.49$ and squares: $x = 46.4$, $S = 3.75$) with the AJH profiles (dashed lines). (*a*) Axial velocity. (*b*) Radial velocity.

each new time step is calculated from (2.9), adopting first-order-accurate forward differencing in time and second-order-accurate central differencing in space, on a 34×514 grid. The vorticity distribution thus computed is used to solve the Poisson equation (2.10) by a Jacobi iterative scheme to obtain the streamfunction everywhere. Numerical acceleration is achieved by a six-level full-multigrid technique (Fletcher 1991). The procedure is repeated until the cumulative change in vorticity reduces to below $= 10^{-10}$.

The axial and radial velocity profiles for $Re_i = 150$ and divergence angle 3° at different downstream locations are compared with the AJH profiles in figures 2(*a*) and 2(*b*) respectively. It is seen that the AJH profile underpredicts the effect of divergence at $x = 22.9$ but overpredicts it at $x = 46.4$. Note that the AJH profiles do not correspond to flow through any particular geometry. At very low angles of divergence, axial variations are slow, the flow attains near-similarity within a short downstream distance, and the AJH profiles are expected to predict the real flow well. We find this to be the case at angles of divergence less than 1°. The profiles computed here are used in the stability calculations, as described in § 3. Incidentally, at higher divergence, regions of separation are obtained to very good accuracy by the present method, but are not the subject of discussion here as our interest is in finding the smallest divergence at which flow behaviour is completely different from that in a straight pipe.

3. Non-parallel stability analysis

We now revert to the use of the local radius $R(x)$ and the local centreline velocity $U_c(x)$ at a given x as scales. Each flow quantity is expressed as the sum of a steady mean and a time-dependent perturbation, such as

$$u = U(x, r) + \hat{u}(x, r, \theta, t). \tag{3.1}$$

Since the flow under consideration varies significantly in the axial direction, a normal mode form may be used only in time and in the azimuthal coordinate θ. In the axial coordinate, the perturbation may be expressed as a rapidly varying wave-like part scaled by a relatively slowly varying function (see e.g. Bertolotti, Herbert & Spalart

https://doi.org/10.1017/S002211200500399X Published online by Cambridge University Press

1992; Govindarajan & Narasimha 1995), such as

$$[\hat{u}, \hat{v}, \hat{w}, \hat{p}] = \mathrm{Re}\left\{ [u(x,r), v(x,r), w(x,r), p(x,r)] \exp\left[\mathrm{i}\left(\int \alpha(x)\,\mathrm{d}x + n\theta - \beta_d t_d \right) \right] \right\}, \tag{3.2}$$

where $\hat{u}$, $\hat{v}$ and $\hat{w}$ are the axial, radial and azimuthal velocity perturbations respectively, $\hat{p}$ is the pressure perturbation, $\alpha(x)$ is a local axial wavenumber, n is the number of waves in the azimuthal direction, and β is the disturbance frequency. Flow quantities in the form (3.1) are substituted in the Navier–Stokes and continuity equations, the mean flow equation is subtracted, and nonlinear terms in the perturbations are neglected. Since axial variations are slow and the Reynolds number is large, a consistent approximation is to retain all terms up to $O(a)$ and $O(Re^{-1})$ (in the critical and wall layers and elsewhere in the pipe) and neglect higher-order effects. The result is a set of partial differential equations for the perturbation velocities and pressure, each of first order in x and up to second order in r, which amounts to a seventh-order system in r. These may be expressed in the form

$$\mathscr{H}\phi(x,r) + \mathscr{G}\frac{\partial \phi(x,r)}{\partial x} = \beta \mathscr{B}\phi(x,r). \tag{3.3}$$

Here $\phi = [u, v, w, p]$, $\beta = \beta_d R/U_c$ and the non-zero elements of the 4×4 matrix operators $\mathscr{H}$, $\mathscr{G}$ and $\mathscr{B}$ are given by

$$h_{11} = U\left[2\frac{U_c'}{U_c} + \mathrm{i}\alpha - ar\frac{\partial}{\partial r}\right] + \frac{\partial U}{\partial x} - ar\frac{\partial U}{\partial r} + V\frac{\partial}{\partial r} + \frac{1}{Re}\left[\alpha^2 + \frac{n^2}{r^2} - \frac{1}{r}\frac{\partial}{\partial r} - \frac{\partial^2}{\partial r^2}\right],$$

$$h_{12} = \frac{\partial U}{\partial r}, \quad h_{14} = \left(2\frac{U_c'}{U_c} + \mathrm{i}\alpha - ar\frac{\partial}{\partial r}\right),$$

$$h_{22} = V\frac{\partial}{\partial r} + \frac{\partial V}{\partial r} + U\left[\frac{U_c'}{U_c} + \mathrm{i}\alpha - ar\frac{\partial}{\partial r}\right] - \frac{1}{Re}\left[\frac{\partial^2}{\partial r^2} + \frac{1}{r}\frac{\partial}{\partial r} - \frac{(1+n^2)}{r^2} - \alpha^2\right],$$

$$h_{23} = \frac{2}{Re}\frac{\mathrm{i}n}{r^2}, \quad h_{24} = \frac{\partial}{\partial r}, \quad h_{32} = -\frac{2}{Re}\frac{\mathrm{i}n}{r^2},$$

$$h_{33} = V\frac{\partial}{\partial r} - \frac{V}{r} + U\left[\frac{U_c'}{U_c} + \mathrm{i}\alpha - ar\frac{\partial}{\partial r}\right] - \frac{1}{Re}\left[\frac{\partial^2}{\partial r^2} + \frac{1}{r}\frac{\partial}{\partial r} - \frac{(1+n^2)}{r^2} - \alpha^2\right], \quad h_{34} = \frac{in}{r},$$

$$h_{41} = \frac{\mathrm{i}\alpha}{Re}\frac{\partial}{\partial r}, \quad h_{42} = V\frac{\partial}{\partial r} + \frac{\partial V}{\partial r} + U\left(\frac{U_c'}{U_c} + \mathrm{i}\alpha - ar\frac{\partial}{\partial r}\right) + \frac{1}{Re}\left(\frac{n^2}{r^2} + \alpha^2\right),$$

$$h_{43} = \frac{\mathrm{i}n}{Re}\left(\frac{1}{r^2} + \frac{1}{r}\frac{\partial}{\partial r}\right), \quad h_{44} = \frac{\partial}{\partial r}; \qquad g_{11} = g_{22} = g_{33} = g_{42} = U, \quad g_{14} = 1,$$

and

$$b_{11} = b_{22} = b_{33} = b_{42} = \mathrm{i}.$$

Here $U_c' = \mathrm{d}U_c/\mathrm{d}x$.

In equation (3.3), we confirm that if we set a, U_c' and $\partial\phi/\partial x$ to zero, we get the parallel stability equations of Gill (1973) and Lessen *et al.* (1968). The boundary conditions emerge from requiring that all quantities vary continuously with r at the centreline (Batchelor & Gill 1962), and obey no-slip at the wall:

$$u = v = w = p = 0 \qquad \text{at } r = 0 \text{ for } n \neq 1, \tag{3.4}$$

https://doi.org/10.1017/S002211200500399X Published online by Cambridge University Press

$$u = p = 0 \quad v + \mathrm{i}w = 0 \qquad \text{at } r = 0 \text{ for } n = 1, \tag{3.5}$$

$$u = v = w = 0 \qquad \text{at } r = 1. \tag{3.6}$$

Note that for $n = 1$, we have only six boundary conditions for a seventh-order system. We therefore generate an extra boundary condition by differentiating the continuity equation with respect to r, and using the fact that $u(x, 0) = 0$, to obtain

$$2\frac{\partial v}{\partial r} + \mathrm{i}n\frac{\partial w}{\partial r} = 0 \qquad \text{at } r = 0 \quad \text{for } n = 1. \tag{3.7}$$

Equation (3.3) may be solved as an eigenvalue problem of larger size (Balachandar & Govindarajan, unpublished) as described below. The streamwise derivative in (3.3) couples neighbouring axial locations in the flow field to one another. Consider two streamwise locations 1 and 2 separated by an incremental distance, i.e. $x_2 = x_1 + \Delta x$. We may write

$$\frac{\partial \phi}{\partial x} = \frac{(\phi_2 - \phi_1)}{\Delta x} + O(\Delta x)^2. \tag{3.8}$$

Since the dimensional freqency β_d remains constant, β_1 and β_2 are related as follows:

$$\kappa \equiv \frac{\beta_2}{\beta_1} = [1 + a\Delta x]\frac{U_{c1}}{U_{c2}}. \tag{3.9}$$

We can therefore write (3.3) as

$$\begin{bmatrix} \mathscr{H}_1 - \mathscr{G}_1/\Delta x & \mathscr{G}_1/\Delta x \\ -\mathscr{G}_2/\Delta x & \mathscr{H}_2 + \mathscr{G}_2/\Delta x \end{bmatrix} \begin{bmatrix} \phi_1 \\ \phi_2 \end{bmatrix} = \beta_1 \begin{bmatrix} \mathscr{B}_1 & 0 \\ 0 & \kappa\mathscr{B}_2 \end{bmatrix} \begin{bmatrix} \phi_1 \\ \phi_2 \end{bmatrix}. \tag{3.10}$$

(Higher-order approximations to the streamwise derivative could be considered instead of (3.8) and the resulting eigensystem would be of correspondingly large size.) The numerical mean flow is interpolated to obtain profiles at neighbouring x-locations, with $\Delta x = 0.05$. Profiles obtained from computations using 512 grid points as well as 1024 grid points have been checked to give eigenvaules correct up to 4 decimal places. Halving or doubling the Δx has even less of an effect on the eigenvalue. Equation (3.10) is solved by a spectral collocation method (Canuto, Hussaini & Quarteroni 1987). The eigenvalue β_1 is obtained as a complex quantity. The complex streamwise wavenumber is iterated until β_1 assumes the desired real value ($= \beta_d R/U_c$) at a given x_1. The axial variation of the wavenumber, $\mathrm{d}\alpha/\mathrm{d}x$, and the initial guess for α_1 are obtained by solving the homogeneous part of (3.3). In subsequent iterations, $\mathrm{d}\alpha/\mathrm{d}x$ is maintained constant, since the correction due to the inhomogeneous terms on this quantity is of higher order. Note that the apportionment in (3.2) between the x-dependences of α and the eigenfunction is arbitrary. There are many ways of performing this apportionment (Bertolotti *et al.* 1992), and so long as the rapid (wave-like) change is included in α_r, there is no difference in the prediction of the growth of any physical quantity. We have checked that this is the case for the present flow as well. Choosing $\mathrm{d}\alpha/\mathrm{d}x$ from the homogeneous part of the equation is one way of including the rapid change into $\alpha(x)$, leaving a relatively slow change in $u(x)$.

We consider downstream growth of disturbances followed at a constant value of the non-dimensional radius r. The growth rate g of the non-dimensional disturbance kinetic energy, $\hat{E} = \frac{1}{2}(\hat{u}^2 + \hat{v}^2 + \hat{w}^2)$, for example, is given by

$$g = \frac{1}{\hat{E}}\frac{\partial \hat{E}}{\partial x} = -2\alpha_i + \frac{1}{E}\frac{\partial E}{\partial x}\Big|_r, \tag{3.11}$$

https://doi.org/10.1017/S002211200500399X Published online by Cambridge University Press

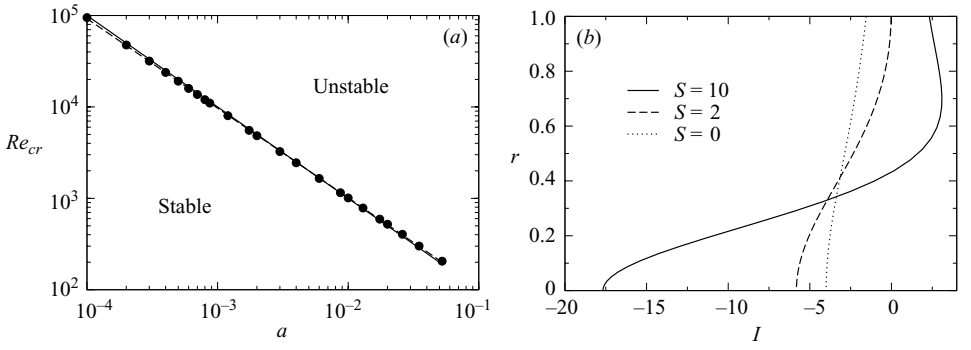


FIGURE 3. (*a*) Variation of the critical Reynolds number with the tangent a of the divergence angle, at small angles of divergence. Symbols: stability analysis; dashed line: best fit; solid line: $Re_{cr} = 10/a$. (*b*) The inviscid instability function I, in straight pipe flow ($S = 0$) and for other values of S.

where $E = \frac{1}{2}(uu^* + vv^* + ww^*)$, the star denotes a complex conjugate. The growth factor for this quantity is thus

$$\frac{E}{E_{cr}} = \exp\left[\int_{x_{cr}}^{x} g(x)\,\mathrm{d}x\right] \tag{3.12}$$

where the subscript cr stands for the critical location, at which $g = 0$. We see that a disturbance may amplify at one r value and decay at another. Secondly, one disturbance quantity could be amplifying while others decay.

4. Results and discussion

The slowest decaying mode in a straight pipe is the swirl mode (of azimuthal wavenumber $n = 1$) (Burridge & Drazin 1969; Corcos & Sellars 1959). In the diverging pipe, we find that this mode again is always the most unstable, and so all results presented here are for $n = 1$. We emphasize that for the 3° divergence, a non-parallel stability analysis is necessary: with a parallel flow assumption, there is no instability until a Reynolds number of about 1000.

We first compare our eigenspectrum for the flow through a straight pipe with that of Schmid & Henningson (2001). Every eigenvalue matches up to the 10th decimal place. Next we study the effect of very small divergence on the stability behaviour by conducting a parallel flow stability analysis (neglecting non-parallel terms in the stability equation) on the AJH profiles. For these parameters, the results have been checked to be the same as those from a non-parallel analysis. Figure 3(*a*) shows the critical Reynolds number for linear instability as a function of the angle of divergence. At small (but non-zero) divergence angle, we find a finite Reynolds number for linear instability. It can be seen that a power-law relationship is obeyed. The best fit of the data gives $Re_{cr} = 11.2a^{-0.98}$, which is practically indistinguishable from $Re_{cr} = 10/a$. The critical Reynolds number thus varies as the inverse of the divergence angle. The inverse relationship arises because an inviscid mechanism is operational at very high Reynolds numbers, and because the AJH velocity profiles (2.8) are described by the product S of Re and a. We thus show that there is a limiting velocity profile corresponding to $S = 10$, and flows where S is greater than 10 are linearly unstable. When the angle of divergence is less than 1°, the AJH profiles are a good approximation of the flow.

https://doi.org/10.1017/S002211200500399X Published online by Cambridge University Press

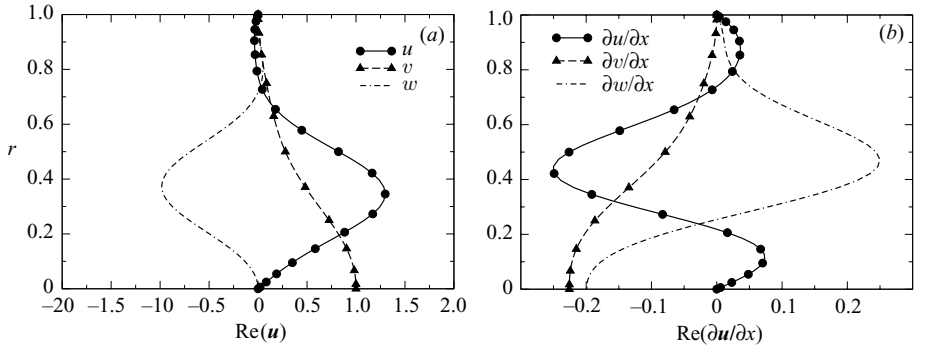


FIGURE 4. (*a*) Eigenfunctions $\boldsymbol{u} = [u, v, w]$ and (*b*) $\partial \boldsymbol{u}/\partial x$ for $Re_i = 150$, $\beta_d = 0.31$ and $n = 1$ at $x_d/R_i = 28.1$.

To understand this behaviour better, we write the equation for inviscid stability (the axisymmetric Rayleigh equation) as the divergence goes to zero, by neglecting terms containing Re^{-1} and a in (3.3), setting $n = 1$, and eliminating w, p and u in turn to obtain

$$(U-c)\left[v'' + \frac{3+\alpha^2 r^2}{1+\alpha^2 r^2}\left(\frac{v'}{r} - \alpha^2 v\right)\right] - \left[U'' - \frac{\alpha^2 r^2 - 1}{r(1+\alpha^2 r^2)}U'\right] v = 0. \tag{4.1}$$

As $r \to \infty$, (4.1), as it should, reduces to the two-dimensional Rayleigh equation. In two-dimensional flow, Rayleigh showed that a necessary condition for instability is that U'' goes through a zero somewhere in the flow (Schmid & Henningson 2001). Several improvements on this criterion have been made for two-dimensional flow. It can be shown that the quantity $I \equiv U'' - (\alpha^2 r^2 - 1)/r/(1+\alpha^2 r^2)U'$ is the axisymmetric analogue in (4.1) of U'' in two-dimensional flow. It may therefore be expected that a change of sign in I within the flow would take the flow closer to instability. Figure 3(*b*) shows the variation of I with the radial coordinate; I undergoes a sign change if $S > 2$, consistent with expectation. A value of $\alpha = 1.26$, corresponding to critical instability, has been used.

We now examine the behaviour at higher levels of divergence. For the geometry shown in figure 1, results from a non-parallel spatial stability analysis (equation (3.10)) performed on the numerically obtained profiles are presented for $Re = 150$ at the inlet. The growth rate, as mentioned before, depends on how far the monitoring location is from the centreline, and on the quantity being monitored. An examination of (3.11) shows that the second term on the right-hand side determines the r-dependence, and comes from the flow quantity under consideration. Typical plots of the eigenfunctions u, v and w, and their axial variations, are shown in figures 4(*a*) and 4(*b*) respectively. The amplitude of the disturbance kinetic energy of the swirl ($n = 1$) mode is shown in figure 5. It is seen that the fastest growth occurs at $r = 0.25$, while the disturbance decays near the wall and near the centreline. Whether this could give rise to structures different from those obtained by Hof *et al.* (2004) needs to be investigated. The Reynolds number is a decreasing function of the axial distance: beyond $x \sim 50$ we find no disturbance that has a positive growth rate. At higher Reynolds numbers, there is scope for turbulent flow in the initial portion of the divergent section, and relaminarization downstream. These aspects are being explored experimentally (A. K. Sood *et al.*, private communication). The sensitivity to small levels of divergence may have implications for small-scale flows.

https://doi.org/10.1017/S002211200500399X Published online by Cambridge University Press

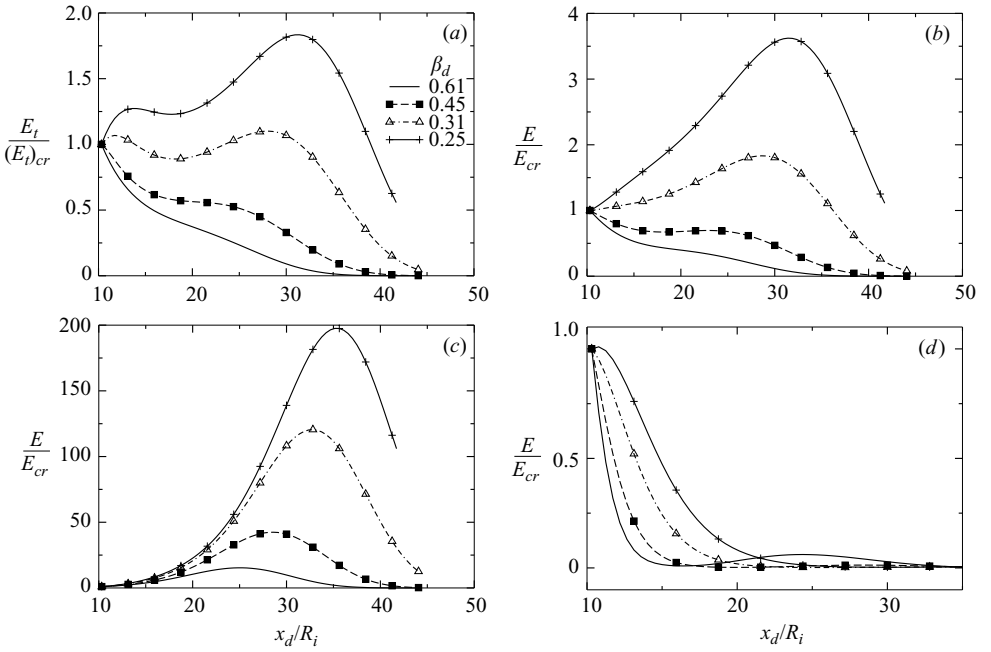


FIGURE 5. Amplification of disturbance kinetic energy for $Re = 150$, $n = 1$ for typical disturbance frequencies. (*a*) Average across the pipe; (*b*) $r = 0.75$; (*c*) at $r = 0.25$; (*d*) at $r = 0.07$. The axial coordinate here is scaled by the inlet radius.

From this study, we cannot tell at what Reynolds number transition to turbulence will be triggered. While an inlet Re of 150 may be too low, it is significant that linear growth has been demonstrated. At $Re = 300$ on the other hand, the disturbance kinetic energy grows by a factor of over 60 000 so a linear mechanism may become important in the transition process. For a continuously diverging pipe, since the Reynolds number is a decreasing function of distance, a relaminarization may occur somewhere downstream, so turbulence could be spatially localized.

In summary, the critical Reynolds number for linear instability of flow in a diverging pipe is finite. For small divergence, instability is determined by the parameter $S(x)$ describing the mean profile, and the mechanism is inviscid. As $a \to 0$, the flow is unstable to the swirl mode for $S > 10$, so the critical Reynolds number approaches infinity as $1/a$. The high rate of disturbance growth at surprisingly low Reynolds numbers indicates that a different route to turbulence from that in a straight pipe is likely. At divergences as low as 1°, the effect of flow non-parallelism is already large, so a non-parallel analysis is essential.

Grateful thanks to George Homsy, Pratap Vanka, Ajay Sood and Narayanan Menon for useful discussions. We thank the DRDO, India, for financial support under ERIP/ER/ 0302109/ M/01/741.

REFERENCES

BATCHELOR, G. K. & GILL, A. E. 1962 Analysis of the stability of axisymmetric jets. *J. Fluid Mech.* **14**, 529–551.

https://doi.org/10.1017/S002211200500399X Published online by Cambridge University Press

Bertolotti, F. P., Herbert, T. & Spalart, P. R. 1992 Linear and nonlinear stability of the Blasius boundary layer. *J. Fluid Mech.* **242**, 441–474.

Burridge, D. M. & Drazin, P. G. 1969 Comments on stability of pipe Poiseuille flow. *Phys. Fluids* **12**, 264–265.

Canuto, C., Hussaini, M. Y., Quarteroni, A. & Zang, T. 1987 *Spectral Methods in Fluid Dynamics*, 1st Edn. Springer.

Cherdron, W., Durst, F. & Whitelaw, J. H. 1978 Asymmetric flows and instabilities in symmetric ducts with sudden expansions. *J. Fluid Mech.* **84**, 13–31.

Corcos, G. M. & Sellars, J. R. 1959 On the stability of fully developed flow in a pipe. *J. Fluid Mech.* **5**, 97–112.

Davey, A. & Drazin, P. G. 1969 The stability of Poiseuille flow in a pipe. *J. Fluid Mech.* **36**, 209–218.

Eagles, P. M. 1965 The stability of a family of Jeffery-Hamel solutions for divergent channel flow. *J. Fluid Mech.* **24**, 191–207.

Eagles, P. M. & Weissman, M. A. 1975 On the stability of slowly varying flow: the divergent channel. *J. Fluid Mech.* **69**, 241–262.

Faisst, H. & Eckhardt, B. 2003 Travelling waves in pipes. *Phys. Rev. Lett.* **91**, 224502.

Faisst, H. & Eckhardt, B. 2004 Sensitive dependence on initial conditions in transition to turbulence in pipe flow. *J. Fluid Mech.* **504**, 343–352.

Fearn, R. M., Mullin, T. & Cliffe, K. A. 1990 Nonlinear flow phenomena in a symmetric sudden expansion. *J. Fluid Mech.* **221**, 595–608.

Fletcher, C. A. J. 1991 *Computational Techniques for Fluid Dynamics*, Vol. I, 2nd Edn. Springer.

Floryan, J. M. 2003 Vortex instability in a diverging-converging channel. *J. Fluid Mech.* **482**, 17–50.

Gill, A. E. 1973 The least-damped disturbance to Poiseuille flow in a circular pipe. *J. Fluid Mech.* **61**, 97–107.

Govindarajan, R. & Narasimha, R. 1995 Stability of spatially developing boundary layers in pressure gradients. *J. Fluid Mech.* **300**, 117–147.

Hof, B., van Doorne, C. W. H., Westerweel, J., Nieuwstadt, F. T. M., Faisst, H., Eckhardt, B., Wedin, H., Kerswell, R. R. & Waleffe, F. 2004 Experimental observation of nonlinear traveling waves in turbulent pipe flow. *Science* **305**, 1594.

Hof, B., Juel, A. & Mullin, T. 2003 Scaling of the turbulence transition threshold in a pipe. *Phys. Rev. Lett.* **91**, 244502.

Huerre, P. & Rossi, M. 1998 Hydrodynamic instabilities in openflows. In *Hydrodynamics and nonlinear instabilities* (ed. C. Godreche & P. Manneville), pp. 81–288. Cambridge University Press.

Lessen, M., Sadler, S. G. & Liu, T. Y. 1968 Stability of pipe Poiseuille flow. *Phys. Fluids* **11**, 1404–1409.

Meseguer, A. & Trefethen, L. N. 2003 Linearized pipe flow to Reynolds number 10^7. *J. Comput. Phys.* **186**, 178–197.

Reynolds, O. 1883 An experimental investigation of the circumastances which determine whether the motion of water shall be direct or sinuous and of the law of resistance in parallel channels. *Phil. Trans. R. Soc. Lond.* **174**, 935–982.

Schmid, P. J. & Henningson, D. S. 1994 Optimal energy density growth in Hagen-Poiseuille flow. *J. Fluid Mech.* **277**, 197–225.

Schmid, P. J. & Henningson, D. S. 2001 *Stability and Transition in Shear Flows*. Springer.

Sreenivasan, K. R. & Strykowski, P. J. 1983 An instability associated with a sudden expansion in a pipe flow. *Phys. Fluids.* **26**, 2766–2768.

Waleffe, F. 1998 Three-dimensional coherent states in plane shear flows. *Phys. Rev. Lett.* **81**x, 4140–4143.

Waleffe, F. 2001 Exact coherent structures in channel flow. *J. Fluid Mech.* **435**, 93–102.

https://doi.org/10.1017/S002211200500399X Published online by Cambridge University Press